Available online at www.sciencedirect.com
SCIENCE DIRECT
Polymer 47 (2006) 5643–5656
polymer
www.elsevier.com/locate/polymer

Influence of molecular composition on the development of microstructure from sheared polyethylene melts: Molecular and lamellar templating

Y. An [a], J.J. Holt [a], G.R. Mitchell [a,*], A.S. Vaughan [b]

[a] JJ Thomson Laboratory, University of Reading, Whiteknights, Reading RG6 6AF, UK
[b] ECS, University of Southampton, Highfield, Southampton SO17 1BJ, UK

Received 14 April 2005; received in revised form 10 January 2006; accepted 13 January 2006
Available online 19 May 2006

Dedicated to Professor David Bassett.

Abstract

A combination of in situ and ex situ X-ray scattering techniques and transmission electron microscopy has been used to study the crystallization behaviour of polyethylene, following the imposition of melt shear. In the case of a branched material, the imposition of shear flow up to a rate of 30 s^{-1} was found to induce no anisotropy. Although shearing the linear material only ever induced a very small degree of anisotropy in the melt, for shear rates >0.15 s^{-1}, subsequent crystallization resulted in increasing anisotropy. Blends of the above two polyethylenes were produced, in which the linear material constituted the minority fraction ($\sim$10%). Isothermal crystallization at temperatures where extensive crystallization of the branched material does not occur demonstrated that the behaviour of the linear component of the sheared blend mirrored that of the linear polyethylene alone. However, in addition, it was found that when crystallized in the presence of an oriented morphology, the branched polymer also formed anisotropic structures. We have termed the process templating, in which the crystallization behaviour of the bulk of the system ($\sim$90% branched material) is completely altered (spherulitic to oriented lamellar) by mapping it onto a pre-existing minority structure ($\sim$10% linear polymer).
© 2006 Elsevier Ltd. All rights reserved.

Keywords: Polyethylene; Shear; Crystallization

1. Introduction

The development of a comprehensive understanding of the crystallization behaviour of polydisperse polymer melts following the imposition of melt flow, represents a major challenge and, consequently, is a topic that has attracted considerable recent attention [1–10]. Whilst it is well appreciated that a degree of molecular variability is required to ensure processability and adequate final properties, the precise role of each molecular fraction in technologically relevant materials is not well understood. Following early studies of extensional flow, which revealed many important general concepts [11–14], it was soon realised that similar structures could also develop from a sheared melt; the characteristic morphology was termed a shish-kebab. At the simplistic level, extension of the longest chains occurs first, in response to the imposed flow field, to give oriented 'shish' structures, which then act as contiguous nucleation sites for the lateral growth of lamellar crystals ('kebabs') [4,15,16] containing shorter molecules. In this process, shish formation is critical, and a range of different interpretations stressing the role of highly oriented molecular segments [17], long-chain/long-chain overlap [5,18], fringed micellelar conformations within the melt [19] and particulate impurities [6] have all been proposed. Indeed, ordered structures have been observed in amorphous sheared isotactic polystyrene, when quenched from the melt [9], and it has even been demonstrated that the addition of high molar mass atactic polypropylene can enhance the nucleation of the isotactic stereo-isomer [20]. Both these observations have led to the suggestion that shish structures are associated with aligned mesomorphic conformations within the melt.

Realistic technological applications of crystallizable polymers exploit materials that contain a broad and continuous spectrum of molecular lengths. Therefore, while fundamental theory is best derived from the study of monodisperse systems, these are not so relevant from a practical perspective. In the case of polyethylene, even when crystallization occurs from

* Corresponding author. Tel.: +44 118 378 8573; fax: +44 118 9750203.
E-mail address: g.r.mitchell@reading.ac.uk (G.R. Mitchell).

0032-3861/$ - see front matter © 2006 Elsevier Ltd. All rights reserved.
doi:10.1016/j.polymer.2006.01.097

a quiescent melt, molecular segregation and fractionation processes often result in complex microstructures, which are both hierarchical and compact [21–23]. To enhance understanding of such complex lamellar textures, blending has often been used to induce morphological simplicity. In this respect, the exploitation of isotactic/atactic blends represents a long-standing strategy [24,25]. In polyethylene, the equivalent involves crystallizing a linear material in the presence of less crystallizable branched polymer [26], where the level of branching limits the thickness of lamellar crystals that is attainable and, therefore, the temperature range within which the polymer can be crystallized. Typically, low density polyethylenes do not crystallize above ~110 °C, whereas linear grades can be crystallized isothermally up to ~130 °C. This, therefore, gives a temperature window of about 20 °C within which the branched polymer effectively acts as a non-crystallizable diluent, such that crystallization of the linear polymer occurs relatively slowly to give simple lamellar textures [27–29]. Although co-crystallization occurs to a degree that is dependent upon the crystallization temperature, it is nevertheless, often convenient to consider the final morphologies in terms of the initial nucleation and growth of lamellae of linear polyethylene (LPE), followed by the separate crystallization of the branched polyethylene (BPE). Our usage of these terms acknowledges that the former can include the more linear segments from the BPE, whilst the latter may include the shortest LPE fraction.

Previously, we have explored the crystallization behaviour of sheared linear polyethylene melts through the strategy of combining real-time, in situ X-ray scattering techniques, with the ex situ examination of larger scale morphologies using transmission electron microscopy (TEM) [30,31]. For the study reported here, we chose, in addition, to exploit the structural simplifications that result from blending a linear polyethylene with a less crystallizable branched material. In such a system, the majority BPE matrix would be expected to behave both as a stress transfer medium and a diluent and, thereby, more clearly reveal the effect of shear flow on crystal nucleation and growth in the minority linear component.

2. Experimental

2.1. Materials

Samples ranging in composition from 0 to 20% LPE were examined during the course of this investigation but, here, we will concentrate on data derived from systems containing 10 or 20% linear plus, respectively, 90 or 80% branched polyethylene. The LPE was supplied by BP Chemicals and exhibits a broad molecular mass range, with $\bar{M}_w = 312,000$ and $\bar{M}_n = 33,000$. The BPE used here is a conventional low density grade produced by Borealis Polymers using a high pressure synthetic route. It is characterised by lower molecular masses ($\bar{M}_w = 76,800$ and $\bar{M}_n = 11,300$) and, in view of its production method, would be expected to contain about 30 branches per 1000 carbon atoms. All the blend samples described here were prepared by solution processing, using xylene as a co-solvent. Appropriate masses of each polymer were first dissolved in xylene at 140 °C to give a 1% w/v solution; the blend was then recovered by precipitation of the polymer in an excess of cold methanol, filtration and vacuum drying.

Specimens for shear experiments were prepared from the above materials by heating the powdered blend in a pre-shaped mould to 160 °C within a laboratory press. Each was held at the final temperature for 5 min and then quenched into water. The mould surfaces were coated with Kapton sheet to facilitate easy specimen removal.

2.2. Thermal analysis

The crystallization and melting behaviour of the above materials was studied, before and after shear, by differential scanning calorimetry (DSC). A Perkin Elmer DSC-2 was used, which was routinely calibrated with high purity indium. Samples of the order of 5 mg in mass were melted at 150 °C and then cooled to 50 °C in the DSC at 10 °C min^{-1}, to obtain non-isothermal crystallization exotherms. The subsequent melting behaviour of these samples was then studied using the reverse thermal ramp (i.e. heating from 50 to 150 °C at 10 °C min^{-1}). Isothermal crystallization experiments were also performed within the temperature range 115–125 °C; that is, at temperatures where the LPE crystallizes but where the BPE acts principally as a non-crystallizable diluent. For these experiments, samples were melted at 150 °C and then cooled rapidly in the DSC to the required crystallization temperature. In the case of previously sheared samples, the time held in the melt at 150 °C was also varied, to explore the effect of melt relaxation on subsequent crystallization kinetics. In all cases, data acquisition and analysis were performed using MC^2 Thermal Systems software.

2.3. Shear cells

Samples approximately 1 mm in thickness were placed into the appropriate parallel plate shear cell, melted at 150 °C and sheared at various shear rates to provide defined shear histories. These samples were then either cooled rapidly (~40 °C min^{-1}) to the required isothermal crystallization temperature, held, and then cooled to room temperature, or cooled to room temperature directly.

Each shear cell was equipped with a small electrically heated oven in which the temperature was controlled using by a Eurotherm three-term proportional-integral-derivative controller. Defined cooling was achieved by the use of a flow of cooled nitrogen gas, together with appropriate electrically operated valves coupled to the Eurotherm controller. Quiescent temperature conditions were calibrated using the melting points of simple organic compounds. The cooling conditions were calibrated by comparing X-ray and DSC data derived from equivalent unsheared samples.

One parallel plate shear cell equipped with mica windows was specially designed to facilitate in situ time-resolving X-ray scattering measurements; the geometry is shown schematically

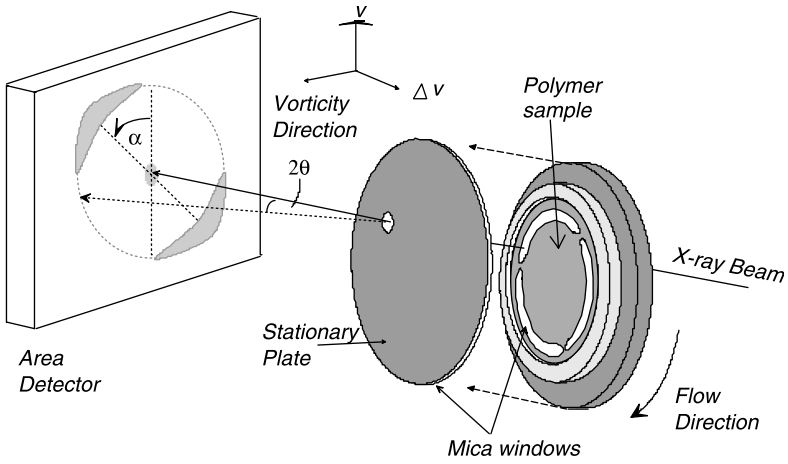

Fig. 1. A schematic diagram of the shear cell used for the in situ time-resolving X-ray scattering measurements described in this work.

in Fig. 1 [32,33]. This shear cell is fitted with plates of diameter 19 mm, which are separated by a gap of 1 mm. The rotating plate consists of a stainless steel tri-spoke arrangement covered with a thin mica disc (0.03 mm in thickness), which allows the incident beam to pass unhindered for 85% of each revolution. An upstream synchronised rotating mask, fabricated from lead, minimises the background intensity for the period of a revolution when a spoke would have intercepted the incident beam. The fixed plate consists of a stainless steel plate with a single chamfered hole covered with a thin mica disc. Pre-moulded samples, prepared as described above, were loaded into the shear cell at room temperature and subjected to a defined heating sequence, which involved ramping to 150 °C at 10 °C min^{-1} and holding for 300 s before commencing shearing. A second shear cell of similar design, but fitted with quartz plates, was used to prepare samples for subsequent room temperature X-ray analysis.

The first shear cell was used together with the intense flux available on the fixed wavelength beam-line 16.1 at the Daresbury Synchrotron Radiation source, to collect time-resolving data using the area X-ray imaging system (AXIS), developed at The University of Reading [34,35]. The AXIS system uses a Photonics Science CCD-based detector system, with a time cycle for data collection and storage of ~1 s. The integrated control and data collection system ensures that each image is time stamped with the appropriate environmental parameters, such as temperature and shear conditions. An incident beam ionization chamber was used to monitor variations in the incident X-ray intensity. Additional steady state measurements were performed in the laboratory using a sealed 1.6 kW X-ray tube with a copper anode.

In both types of experiment, the scattering vector relating to the features of principal interest (the {110} polyethylene Bragg peaks), lay at an angle of ~10° to the plane containing the flow and vorticity vectors. The small X-ray beam diameter of ~0.3 mm enabled the diffraction patterns to be obtained from defined volumes of material, which had been subjected to an effectively constant shear rate (±1%). The shear rates quoted in the text are the values calculated for the radius corresponding to the centre of the irradiated area.

The pixel size and uniformity of the detector was calibrated using a series of masks with defined aperture arrays. The effective sample to detector distance was calibrated using a highly crystalline sample of polyethylene. The centre of the diffraction pattern was found using the symmetry inherent in the pattern from an isotropic sample. In this way, quantitative pixelated scattering patterns $I(|Q|,\alpha)$ could be obtained, where $|Q| = (4\pi \sin\lambda)/\lambda$, λ is the relevant incident X-ray wavelength, 2θ the scattering angle and α the angle between the flow axis and the projection of the scattering vector Q onto the plane of the detector. Azimuthal sections (i.e. scattered intensity as a function of α) at constant $|Q|$ were extracted using the pixels located within an annulus corresponding to the selected $|Q|$ with a width of ΔQ of 0.02 $Å^{-1}$. The sections extracted were normalized using the solid angle subtended by each pixel that contributed to a particular $|Q|$ value. Variations in the detector response and the partial polarization of the incident beam were corrected for using an equivalent section obtained from an isotropic sample (molten polymer). The data from the incident beam monitor was employed to correct the scattered intensities for variations in the incident beam. Azimuthal sections obtained in this manner were used to monitor the level of preferred orientation of the {110} and {200} polyethylene crystal planes. Where a quantitative measure of orientation was required, we evaluated the full width at half maximum (FWHM) of the azimuthal variations by fitting the observed data with Gaussian peaks (as a function of α) and a constant (with respect to α) level signal, using the standard Levenberg–Marquardt non-linear least-squares methodology.

Radial sections (i.e. scattered intensity as a function of $|Q|$) were obtained in a similar manner to that described above, using the pixels located within a wedge of constant $\Delta\alpha = 10°$. Again, data were normalized to account for incident beam variations and the solid angle subtended by each pixel. The section was not corrected for radial variations in the detector response; previous calibrations of the detector had shown that such radial variations are smoothly varying and close to linear, with a maximum correction of ~20%. Corrections to account for the effects of absorption, sample volume and multiple scattering were not made for this series of comparative

experiments, as the geometry and material factors remained constant throughout. To monitor the process of crystallization, we plotted the intensity taken from a radial section at the value of $|Q|$ corresponding to the position of the {110} polyethylene crystal reflection. Although this intensity value will contain contributions from both crystalline and non-crystalline components, in this work, we simply used this parameter as a monitor of crystallization and no particular ambiguities arose.

2.4. Morphology

The internal morphology of a range of samples was examined in the TEM, following permanganic etching [36–38]. Samples were typically etched for 4 h using a 1% solution of potassium permanganate dissolved in an acid mix containing 5 parts concentrated sulphuric acid to 2 parts orthophosphoric acid to 1 part water. This procedure removes sufficient material from the samples to eliminate any surface specific morphologies. After etching, samples were replicated using a standard two stage replication procedure [39]; care was taken to ensure that replicas were taken from areas equivalent to those from which X-ray data were collected (i.e. at the same radial distance from the centre of the sample). All replicas were shadowed radially and examined using a Philips EM301 operating at 80 kV.

3. Results

3.1. DSC behaviour

Fig. 2 illustrates the crystallization and melting behaviour of the LPE and BPE materials, together with that of a blend containing 10% LPE. Fig. 2(a) contains three non-isothermal crystallization exotherms, from which it is apparent that both the LPE and the BPE, in isolation, exhibit singular crystallization peaks (LPE: peak temperature 119 °C; BPE: peak temperature 98 °C). Conversely, the blend system is characterized by two transitions; the LPE crystallizes first at 110 °C, the BPE crystallizing later at 100 °C. The crystallization behaviour of blends of linear and branched polyethylene from quiescent melts has been reported by many workers (see, for example, [27–29]); the DSC results, shown in Fig. 2(a), are in line with expectations and indicate that the difference in crystallization temperature between our BPE and LPE materials is ~20 °C. Thus, ignoring co-crystallization effects, these results suggest that there is a temperature window between about 110 and 130 °C in which it is possible to crystallize only the LPE. However, more detailed studies indicate that, in practice, varying degrees of co-crystallization will occur throughout this range [40]; evidence of this can be seen in the DSC melting trace of the blend specimen in Fig. 2(b), where the LPE melting endotherm takes the form of a double peak. During crystallization, the more linear segments from the BPE are incorporated into some of the isothermally formed, LPE-rich lamellae, such that this fraction of the isothermal crystal population is unable to anneal and thicken during the DSC scan. The observed double melting peak is the result [40].

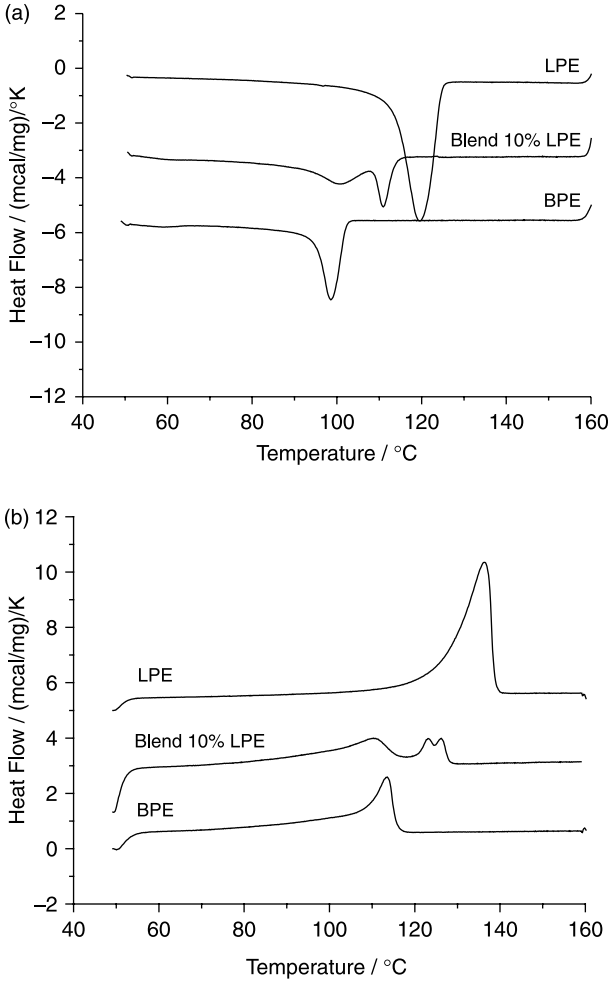

Fig. 2. DSC crystallization and melting traces derived from the linear polyethylene, a blend containing 10% LPE and 90% BPE and the branched polymer: (a) non-isothermal crystallization exotherms recorded at a cooling rate of 10 °C min^{-1} and (b) subsequent melting endotherms recorded at 10 °C min^{-1}.

If the effect of shear on crystal nucleation and growth is to be revealed by experiments where the melt is sheared, shearing stops and, only then, does crystallization begin, it is essential that the melt retains a memory of the imposed shear history for times in excess of those required for crystallization to occur [19,41]. To explore the effect of shear and subsequent melt relaxation on crystallization behaviour, a number of preliminary experiments were, therefore, performed, in which samples were sheared at a rate of 25 s^{-1} for 20 s, quenched immediately and then examined by DSC. In the text that follows, the term 're-crystallized' is used to reinforce the fact that these samples have been sheared, quenched, and momentarily remelted prior to the acquisition of the crystallization data that are shown.

Fig. 3 compares the isothermal re-crystallization behaviour of a sample containing 10% LPE that had previously been sheared and quenched as described above, with the crystallization behaviour of an equivalent unsheared specimen. Both

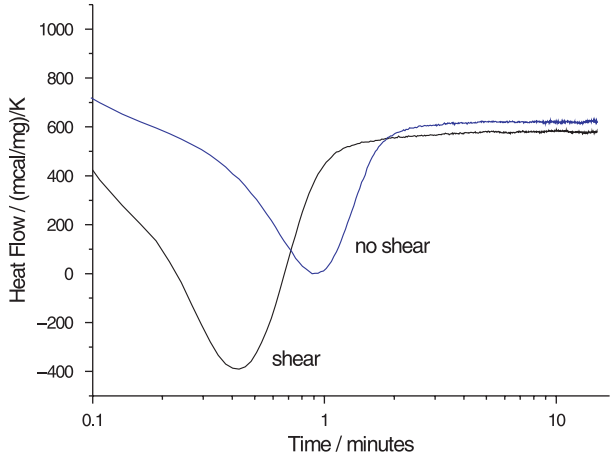

Fig. 3. Isothermal DSC crystallization and re-crystallization exotherms showing the effect of prior shear on the crystallization behaviour of a polyethylene blend containing 10% LPE and 90% BPE at 115 °C. The trace labelled shear was derived from a specimen that had previously been sheared for 20 s at 150 °C and a shear rate of 25 s^{-1}.

were melted momentarily at 150 °C before being crystallized at 115 °C. In the absence of any prior shear, the peak maximum in the crystallization exotherm occurs about 0.8 min after the DSC indicates that the sample temperature has stabilized at 115 °C; for this system, the crystallization process is complete after about 2 min. From the position of the re-crystallization exotherm obtained from the previously sheared sample, it is clear that shearing has resulted in a significant increase in the overall crystallization rate [42]. Although it has been claimed that shearing can serve to increase crystal growth rates [43], most authors have assumed constant crystal growth rates, certainly after cessation of flow. Thus, in line with the majority of previous studies [4,10,44], we interpret this increase in the overall rate of crystallization as being indicative of enhanced nucleation.

Fig. 3 leads to the following conclusions. First, that a memory of the shear history of the sheared sample has indeed been retained and second, by implication, that the overall rate of crystallization provides a convenient indicator by which to explore melt relaxation processes. Evidently, melt relaxation will eventually erase memory of the shear flow and, therefore, to examine this more quantitatively, a series of samples, sheared as above, were held in the melt at 150 °C for varying times and then crystallized at 115 °C. Fig. 4 contains a plot of isothermal re-crystallization time at 115 °C, as represented by the maximum in the DSC exotherm, against holding time in the melt. From this, it is evident that the re-crystallization time increases progressively as the system relaxes, to approach asymptotically the behaviour of the unsheared specimen in Fig. 3. Thus, it would appear that some 2 h relaxation at 150 °C is required to remove all memory of shearing from this system and, consequently, we conclude that melt relaxation will not have a major influence on the subsequent crystallization behaviour of our materials, provided this occurs on a time scale of the order of a few minutes.

Fig. 5 contains a series of re-crystallization exotherms derived from samples isothermally re-crystallized at various

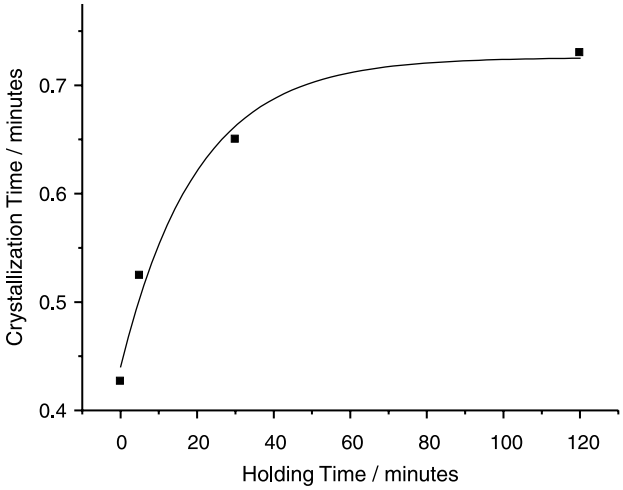

Fig. 4. Plot of isothermal re-crystallization time at 115 °C (peak in the crystallization exotherm) against melt relaxation time at 150 °C.

temperatures, again after initially being sheared at 25 s^{-1} for 20 s and quenched. The position of the peak maximum in the re-crystallization exotherm (arrowed) occurs at times ranging from ~0.4 min at 115 °C to ~4 min at 120 °C, indicating that only at temperatures above 122 °C, is the total re-crystallization time sufficiently long that molecular relaxation in the melt could impact significantly upon crystallization processes.

3.2. Ex situ X-ray studies of samples crystallized from sheared melts

A range of samples was initially prepared by subjecting each specimen to shear flow at 150 °C for such a time that the product of shear rate and time exceeded 100 shear units. After this, the shear flow was stopped and the sample rapidly cooled to room temperature. Fig. 6 shows X-ray patterns obtained from the LPE, each pattern is accompanied by plots of the azimuthual distribution of intensity at scattering angles corresponding to the {110} and {200} polyethylene crystal

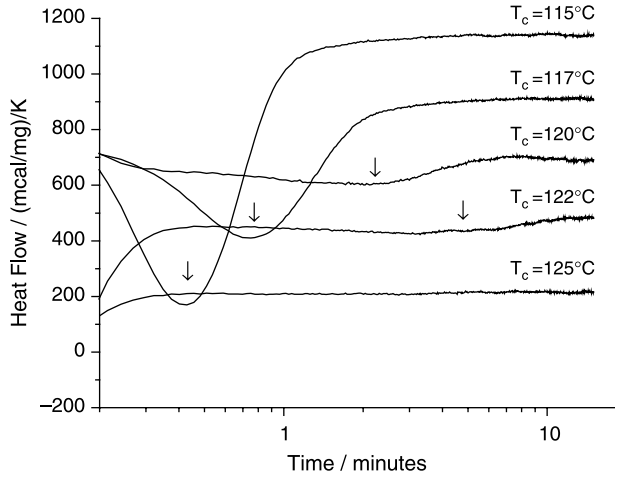

Fig. 5. Isothermal DSC re-crystallization exotherms obtained from blend samples previously sheared for 20 s at 150 °C and a shear rate of 25 s^{-1}. The re-crystallization temperature for each trace is as indicated.

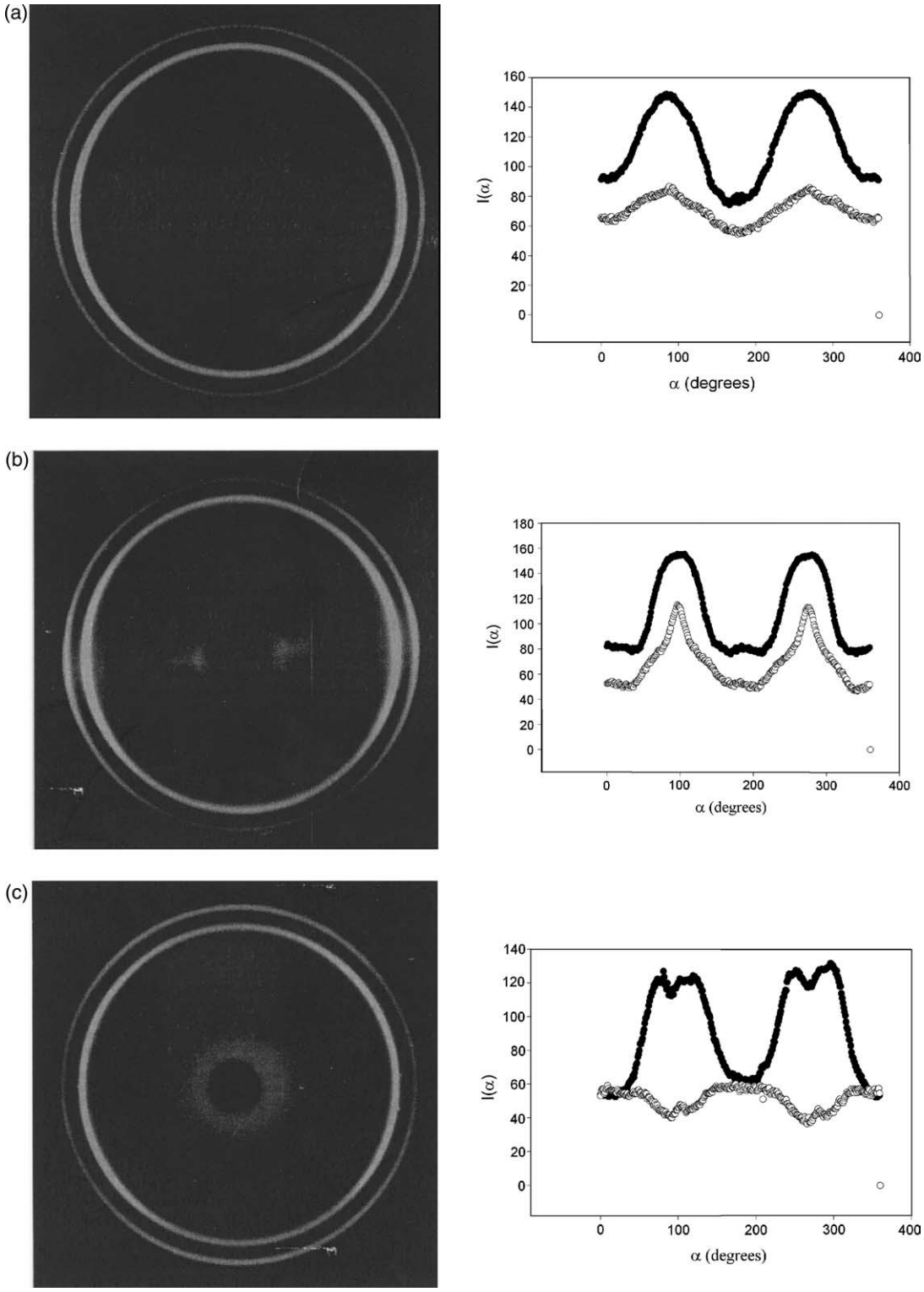

Fig. 6. Ex situ X-ray scattering patterns and derived azimuthal intensity data showing the effect of melt shear rate on anisotropy in quenched LPE. All specimens were sheared at 150 °C for a total of 100 shear units: (a) at a shear rate of 0.06 s^{-1}; (b) at a shear rate of 0.17 s^{-1}; (c) at a shear rate of 11.4 s^{-1}. In the scattering patterns, the flow direction corresponds to the vertical direction on the page while, in the azimuthal scans, $\alpha = 0$ corresponds to the situation where the scattering vector is approximately parallel to the flow direction. ({110} ● {200} ○).

peaks. For a lamellar crystal system, this distribution of intensity will depend both upon both the preferred orientation of the lamellae and the distribution of crystal planes within the lamellae. This problem was first studied by Keller [45,46] who identified that patterns of the type shown in Fig. 6(c), in which the {110} reflection appears as maxima offset from the equator while the {200} reflection is most intense on the meridian, arise from lamellae that have grown in a direction normal to the

{010} face of the crystal and which twist about that direction. More recent work [47] has shown that such patterns can also be obtained from a system in which the constituent lamellae are tilted at a range of angles with respect to the growth axis. Under different preparation conditions, the fibre-like pattern shown in Fig. 6(b) may be obtained. In this, the two reflections are most intense on the equator, indicating that the crystalline chains are then largely parallel to the flow axis. If we examine the azimuthal pattern in Fig. 6(c) in more detail, we see that the profile for the {200} peak contains both small equatorial features and broad meridional maxima. In a similar manner, the {200} profile in Fig. 6(b), contains relatively sharp equatorial features together with rather broad features, also centred on the equator. The profiles in Fig. 6(a) appear to be less defined versions of those seen in Fig. 6(b).

We can now compare the above patterns, which were obtained from samples that had been crystallized from melts sheared at different rates but the same shear strain. Clearly, to extract the precise level of lamellar orientation from these profiles is challenging, as it will depend upon the range of lamellar tilts that exist within each sample. Nevertheless, it is straightforward to identify that the qualitative level of preferred orientation is less in samples prepared at low shear rates ($0.06\ s^{-1}$ in Fig. 6(a)), which is sufficient within the context of this study. As we move to samples prepared by crystallizing melts that had been subjected to higher shear rates, there are increases in preferred orientation (for example, Fig. 6(b) and (c)). The observation that the formation of highly oriented structures occurs above a particular shear rate ($\sim 0.15\ s^{-1}$ here) is, qualitatively in line with the work of Kornfield and co-workers on polypropylene [5,18] and our previous studies of linear polyethylene [30,31]. However, the results presented here do differ from our earlier work in two significant respects:

(i) Previously, the onset of oriented crystallization appeared at $\sim 1\ s^{-1}$ whereas, in Fig. 6, a degree of anisotropy is apparent at lower shear rates. We note that some authors have discussed their results in terms of a critical shear strain [8], while others have suggested the existence of a critical shear stress [10].
(ii) Here, all samples experienced the same shear strain (100 shear units) whereas, previously, all our samples were sheared for the same time.

Undoubtedly, it is this second factor, which accounts for the difference in the onset of orientation and suggests that the subsequent process of crystallization is not a consequence of deformation of an entangled molecular network but, rather, is associated with a balance between molecular orientation and relaxation within the melt [4]. Thus, for a given material, both shear rate and shear strain are important in the formation of oriented crystalline morphologies; network deformation would, more likely, require only a critical shear rate.

Fig. 7 compares equivalent X-ray data obtained from the BPE and a blend system; both scattering patterns were obtained from samples sheared at $10\ s^{-1}$ and, consequently, are comparable with the data shown in Fig. 6(c). The BPE scattering pattern shows no evidence whatsoever of anisotropy and this typified every sample of this polymer that we studied; that is, up to a shear rate of $30\ s^{-1}$. Spherulitic crystallization in two different linear low density polyethylene systems ($\bar{M}_w \sim 10^5$) sheared at rates of up to $18\ s^{-1}$ has previously been reported by Chai et al. [8].

In view of our BPE data and the consistent results of Chai et al. [8], the behaviour of the quenched blend, shown in Fig. 7(b), is somewhat surprising. Despite containing 90% BPE, the crystallized blend sample nevertheless exhibits considerable anisotropy. Indeed, on the basis of the azimuthal distribution of intensity of the {110} and {200} reflections, this blend system appears to highly oriented, in a similar manner to the equivalent LPE sample discussed above. The azimuthal distributions of intensity for the {110} and {200} reflections in Fig. 7(b) are comparable to the pattern and profile shown in Fig. 6(c) for the LPE. The {110} profile (Fig. 7(b)) shows that it contains two pairs of two overlapping peaks symmetrically distributed about the equatorial section, such that each peak is offset from the equator by $\sim 20°$. It is difficult to identify any equatorial component in the 200 profile. In other words the pattern contains diffraction features commensurate with a range of lamellar tilts. Indeed, Keller [46] speculated that this type of pattern would occur as the density of row nuclei drops, as would be expected for a system in which relatively low molar mass BPE represents the majority component.

The similarity between the final X-ray scattering behaviour of the LPE and the blend, which contains just 10% LPE, is reinforced in Fig. 8. In this, we have taken the FWHM, $W_{1/2}$, of the peaks offset from the equator in the {110} azimuthal profile as a measure of the preferred orientation and plotted the results against the prior shear rate. These data were all obtained from samples sheared and then quenched. In the LPE case, the width initially drops as the level of preferred orientation increases with shear rate and then remains approximately constant for shear rates above about $0.3\ s^{-1}$. The behaviour of the quenched blend is similar, but displaced to higher shear rates, an effect that is again reasonable in view of the much lower molecular mass of the BPE in this blend. Since the {110} peak width data for the blend include contributions from the BPE and the LPE, the fact that the behaviour of the blend is so similar to that of the LPE strongly suggests that, in the former system, both the BPE and LPE are incorporated into oriented structures. This is despite the clear result that, in isolation, the BPE exhibits no anisotropy whatsoever, over the complete range of shear conditions used in this study.

3.3. In situ X-ray studies of crystallization from sheared melts

To study the effect of melt shear on the subsequent crystallization behaviour of the blend, time resolving X-ray scattering patterns were recorded throughout the isothermal crystallization process. Although data were gathered at a number of different temperatures using specimens with varying molecular compositions, here we will concentrate on just one example.

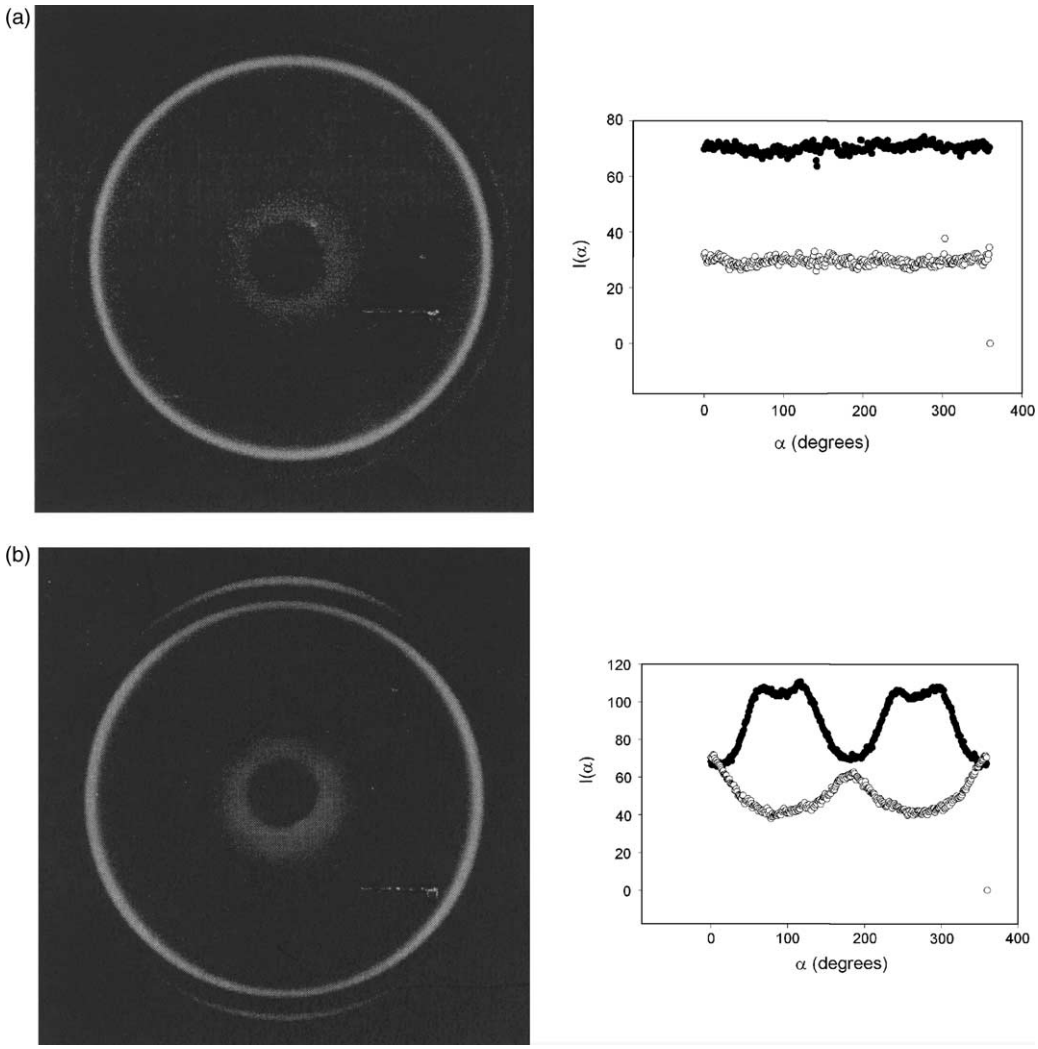

Fig. 7. Ex situ X-ray scattering patterns and derived azimuthal intensity data comparing the effect of shear (150 °C; 100 shear units; 10.0 s^{-1}) on the crystallization behaviour of (a) quenched BPE and (b) a quenched blend containing 10% LPE and 90% BPE. In the scattering patterns, the flow direction corresponds to the vertical direction on the page while, in the azimuthal scans, $\alpha = 0$ corresponds to the situation where the scattering vector is approximately parallel to the flow direction. ({110} ● {200} ○).

Fig. 9 shows a series of diffraction patterns obtained from a blend sample containing 20% LPE and 80% BPE. The increase in linear content from the 10% LPE system considered above results in an improved signal to noise ratio but, otherwise, 10 and 20% LPE blends behave in an equivalent manner. Each pattern was obtained by averaging over a time-slice of about 7 s. The scattering pattern of the melt, after shearing for 120 s at a shear rate of 20 s^{-1}, is shown in Fig. 9(a), in which a uniform, diffuse scattering ring, typical of a molten polymer, can be seen. The dark 'lollipop' shape at the centre of the diffraction pattern is the beam stop placed in front of the detector. As reported previously, an intermediate shear history such as this induces very little anisotropy in the melt [30]. Fig. 9(b') shows the earliest stage of crystallization at ~115 °C. Weak equatorial {110} arcs can just be seen which, as crystallization proceeds, increase in intensity; the pattern obtained in the following time-slice is shown in Fig. 9(b). To facilitate visualisation of the weak diffraction features, the diffraction pattern obtained from the melt

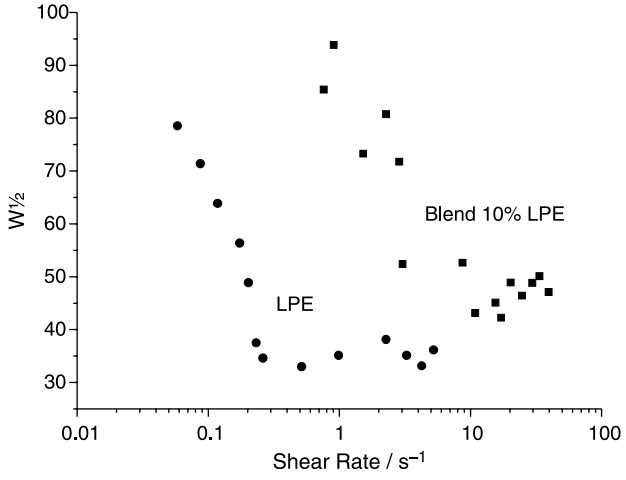

Fig. 8. Plots of the equatorial {110} FWHM, $W_{1/2}$, against shear rate (100 shear units at 150 °C) for the LPE (circles) and a blend containing 10% LPE and 90% BPE (squares).

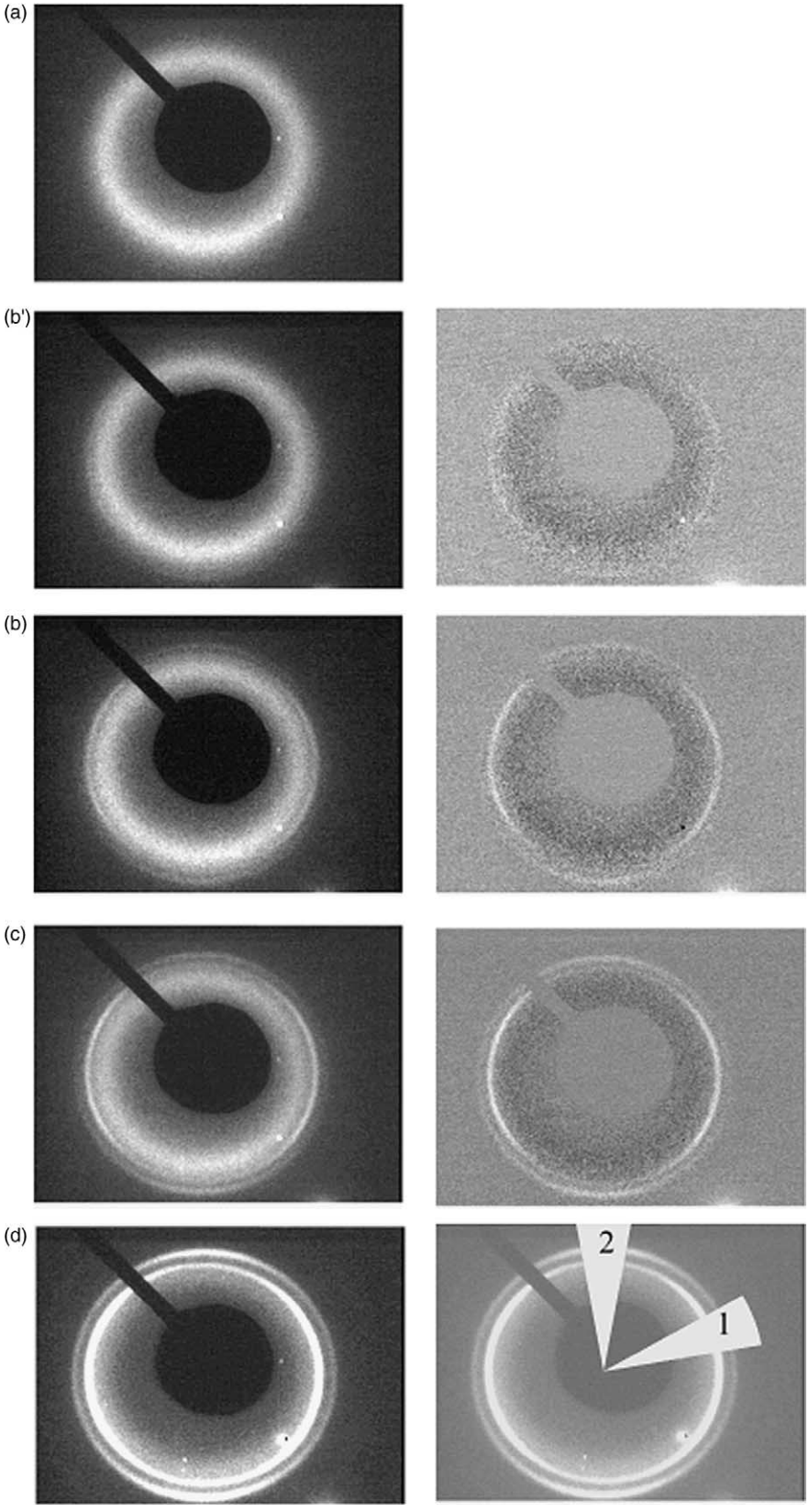

Fig. 9. In situ, time-resolving X-ray scattering patterns following the crystallization process in a blend containing 20% LPE and 80% BPE. The scattering patterns were obtained (a) from the melt immediately after shearing for 120 s at a shear rate of 20 s^{-1}, (b') at the onset of isothermal crystallization at 115 °C (b) just after the onset of isothermal crystallization at 115 °C, (c) at the end of isothermal crystallization at 115 °C and (d) following quenching. Each difference pattern in the right-hand column was obtained by subtracting pattern (a), obtained from the melt, from the corresponding diffraction pattern on the left. In all cases, the flow direction corresponds to the vertical direction on the page.

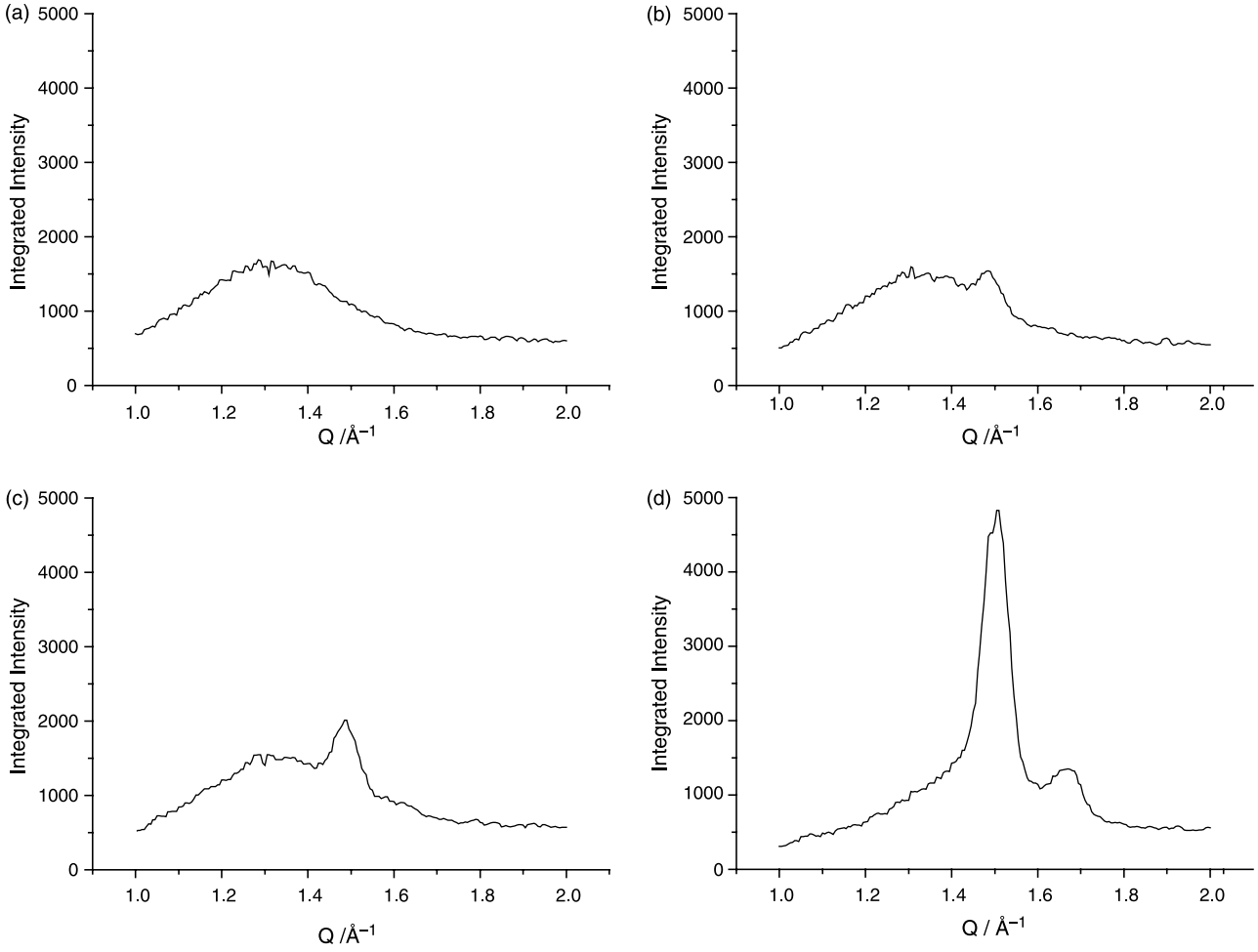

Fig. 10. Equatorial sections obtained from the diffraction patterns shown in Fig. 9, using the section labelled 1. The labelling a, b, c and d also corresponds to that used in Fig. 9.

(Fig. 9(a)) has been subtracted from each of these patterns; the resulting difference patterns are shown in the right-hand column of Fig. 9. In these, the dark diffuse ring on the inside of the sharp arcs is an artefact resulting from differences in the melt pattern due to the change in temperature and the reduction in the amorphous component that results from crystallization. Despite such effects, it can be seen that each difference pattern consists of two diffraction rings; the inner contains four peaks distributed around the equator, but each offset from it by ~20°, while the outer ring is most intense close to the meridonal axis. This pattern is typical of a system of lamellae with a preferred growth direction that is oriented largely perpendicular to the initial flow direction, as we have already seen in Fig. 7(b) [45–47]. The extent of arcing represents the degree to which these lamellae share a common growth direction. Fig. 9(c) shows the maximum intensity attained at the isothermal crystallization temperature; that is, after all the material that is crystallizable at 115 °C has crystallized. Finally, Fig. 9(d) contains the scattering pattern obtained after quenching.

From each of the patterns (a, b, c and d) in the left-hand column of Fig. 9, we have extracted equatorial and meridional sections, which are, respectively, shown in Figs. 10 and 11 to illustrate more quantitatively the increasing level of crystallinity and anisotropy as both time and temperature change. Also, the intensity within the equatorial section corresponding to the position of the {110} reflection has been calculated for each of the diffraction patterns obtained in a complete experiment and plotted as a function of time (Fig. 12), together with the sample's temperature profile. Here, $t=0$ corresponds to the point at which the shear flow ceased and the cooling stage to the isothermal crystallization temperature of ~115 °C was initiated. Thus, the intensity at (a) in Fig. 12 corresponds to the diffuse scattering from the melt while the subsequent increase to a plateau value of ~1700 can be attributed to the developing level of crystallinity during the isothermal LPE crystallization stage. From this variation in intensity, the level of crystallinity present in samples corresponding to Fig. 9(b') and (b) can be estimated. Clearly, it is very small indeed. Upon cooling to room temperature, the integrated intensity increases substantially, by an additional ~3300 units. These steps are in the proportion expected for the ratio of the LPE and BPE components present in the sample. Clearly, the absolute intensities have increased as a result of crystallization of the BPE; time resolving small angle X-ray scattering experiments on 50:50 LPE:BPE blends imply that this occurs within the initially formed linear lamellar framework [48]. However,

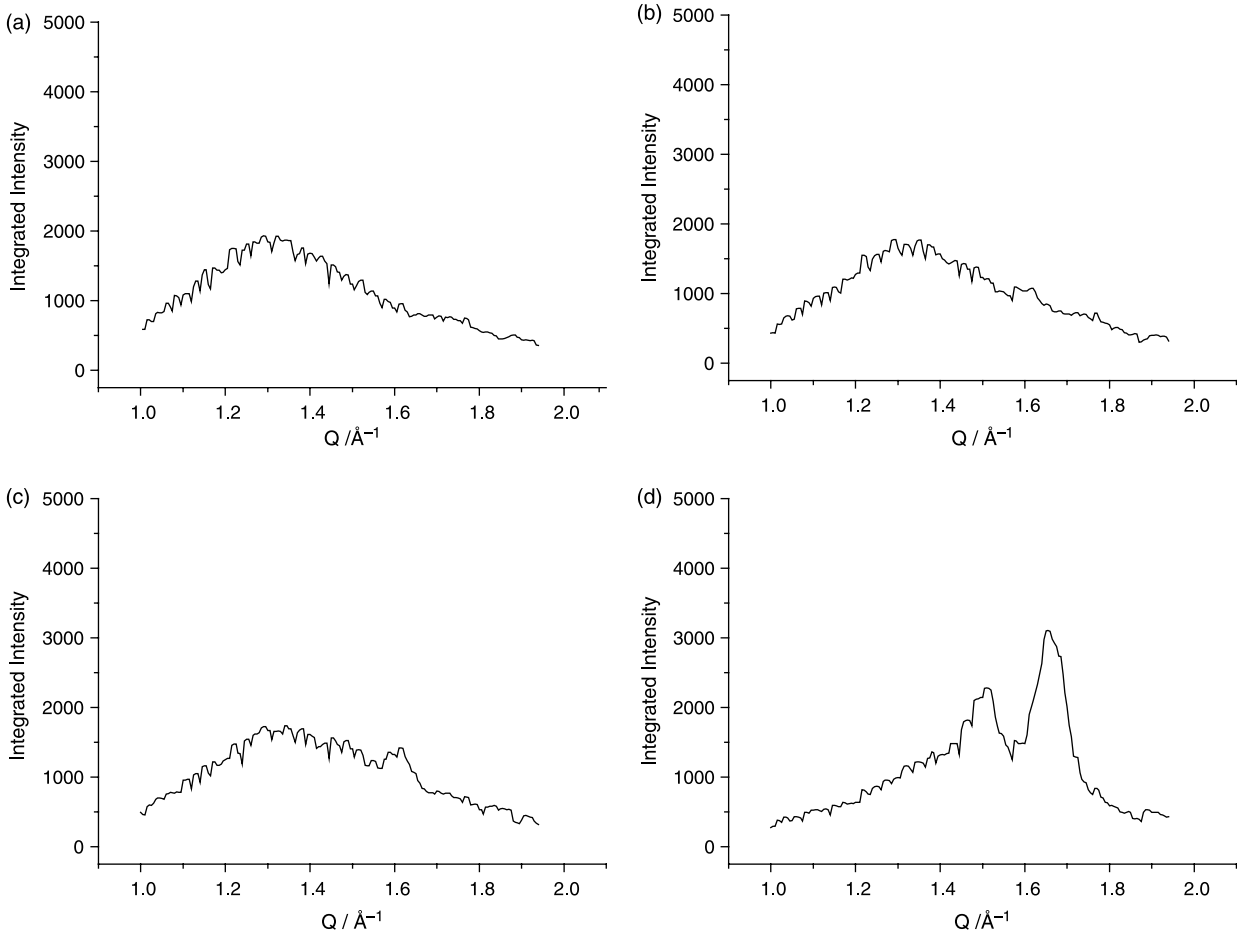

Fig. 11. Meridional sections obtained from the diffraction patterns shown in Fig. 9, using the section labelled 2. The labelling a, b, c and d also corresponds to that used in Fig. 9.

here, the pattern is as anisotropic as that shown in Fig 9(b) and (c), despite the fact that the LPE lamellar framework is unlikely to be space filling in a polyethylene blend of this composition. Moreover the nature of the preferred orientation of the crystal planes, as seen from the azimuthual distribution of intensity in the two diffraction rings, is the same for patterns taken in the very early stages of crystallization (Fig. 9(b') and (b)) as for the final room temperature sample (Fig. 9(d)). Thus, growth of the BPE occurs outside the framework of linear lamellae but, nevertheless, still leads to structures, which, in terms of their molecular anisotropy, appear to mirror the LPE that crystallized isothermally.

3.4. TEM studies of specimens crystallized from sheared melts

The effect of melt shear on the subsequent crystallization process is illustrated in Figs. 13 and 14. Fig. 13(a) shows a high magnification TEM micrograph of an LPE sample that was crystallized by quenching from a quiescent melt. Extensive dominant lamellae can be seen in a range of orientations, separated from one another by much smaller subsidiary crystals [21]. The absence of any larger scale structures, such as spherulites, indicates that, in this material, profuse nucleation occurs on quenching from the melt, which is not unexpected in view of this polymer's relatively high molecular mass. Conversely, the BPE forms well defined spherulitic structures on quenching, the form of which appears independent of any prior shear history. Fig. 13(b) shows a typical BPE spherulitic texture, which is characterized by its somewhat

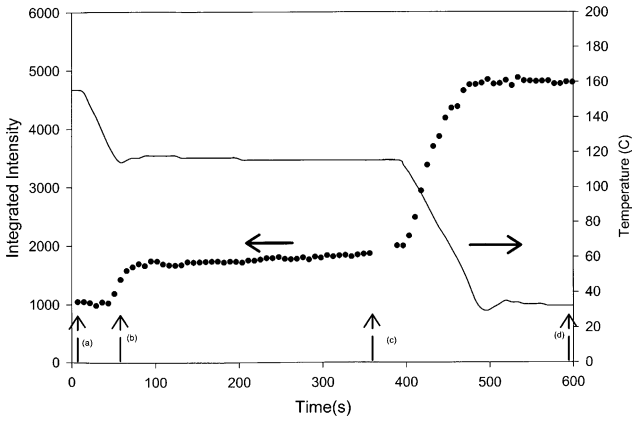

Fig. 12. Plot of X-ray intensity at the position of the {110} diffraction peak as a function of time after cessation of shear (solid circles). The continuous line corresponds to the temperature of the sample recorded during the experiment. The vertical arrows indicate the times at which the patterns show in Fig. 9 were taken; b' was obtained in the time-slice immediately prior to that marked b.

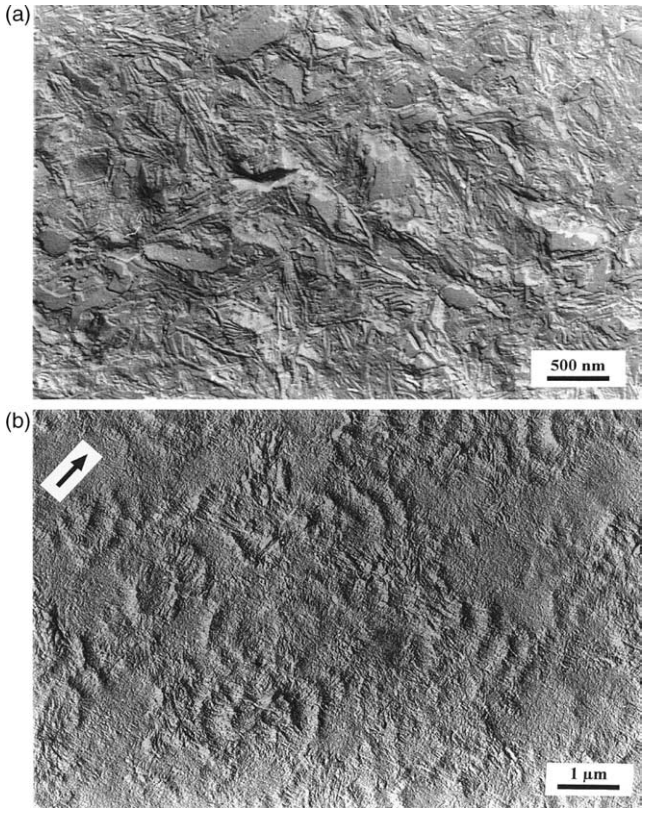

Fig. 13. Representative TEM morphologies seen in (a) quenched LPE crystallized from a quiescent melt and (b) quenched BPE after shearing at 25 s^{-1}.

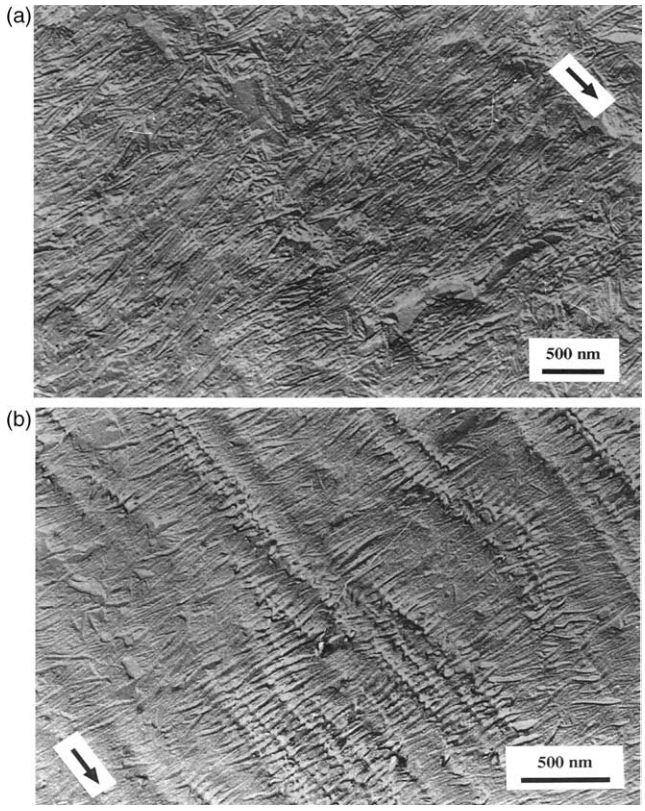

Fig. 14. Representative TEM morphologies seen (a) in quenched LPE and (b) a blend containing 10% LPE and 90% BPE crystallized isothermally at 115 °C. Both samples had been sheared at 25 s^{-1}.

irregular form [49,50]; this texture developed from a melt that had been sheared at 25 s^{-1}, with the shear direction as indicated. The blend system forms similar spherulitic structures when the quiescent melt is quenched, as reported elsewhere [40].

Fig. 14 compares the anisotropic morphologies seen in LPE (quenched) and a 10% LPE blend (crystallized at 115 °C) after shearing at 25 s^{-1}. In the linear system (Fig. 14(a)), shearing results in the formation of compact shish-kebab structures, in which the lamellar over-growths are oriented perpendicular to the core axis. This morphological form closely resembles those described by Hosier et al. [51] as being typical of high strain rates. Such structures develop through a sequential crystallization process; initially, molecules longer than some critical length [1,4] are extended and act as nucleation centres for subsequent chainfolded overgrowth by crystallization of lower molecular mass material [52,53]. Lamellae then grow radially outward, until neighbouring shish-kebabs impinge. In this example, this process has occurred during quenching, but equivalent structures also form under isothermal conditions.

In the blend, similar linear-rich shish-kebabs can be seen, which are, as above, composed of extended cores decorated with relatively thick, isothermal, chainfolded lamellae (Fig. 14(b)). Both of these structural elements formed under isothermal conditions. However, in comparison with the morphology shown in Fig. 14(a), this structure appears much more open, both in terms of the density of isothermal lamellae along each core and with respect to the separation between one shish-kebab and another. Taking Fig. 3(a) at the most simplistic level, the BPE is unable to crystallize at 115 °C and, therefore, the open nature of the morphology visible in Fig. 14(b) is a direct consequence of the lack of material within this blend that is isothermally crystallizable at this temperature. From Fig. 14(b), neighbouring shish-kebabs are, typically separated by ~300 nm and the most extensive lamellar overgrowths are of a similar dimension.

Between the isothermal structures described above is located the BPE material, which crystallized on quenching. From Fig. 14(b), it is evident that the crystals that form on quenching develop such that they are, largely, oriented parallel to the existing isothermal lamellae. This result is, in itself, unexpected. First, this sample was held at 115 °C for 15 min between the termination of shear and quenching (i.e. crystallization of the BPE-rich component); from Fig. 4, this is a sufficient period for significant melt relaxation to occur, even in our relatively high molar mass LPE. Second, even crystallizing the BPE component of this system immediately after shearing resulted in no orientation whatsoever. Thus, we infer that it is the presence of the minority, linear component that is the origin of the orientation of the BPE. Whilst the presence of linear polyethylene lamellae have been reported elsewhere to enhance the crystallization of BPE, this was previously seen under quiescent isothermal conditions where, given sufficient time, the more linear segments within the BPE were able to

co-crystallize along with the LPE [54]. The result is then a modest increase in crystallinity above that which would be expected based upon the simplistic notion of a two-component system in which the BPE acts as a non-crystallizable diluent. We are not aware of any previous studies of such processes in sheared systems, or cases where such dramatic effects have been observed—that is, the minority LPE is serving to modify the complete BPE phase. Also, we believe that the above results have important general implications for the control of microstructure in technological materials that have undergone low-shear processing.

4. Discussion

By combining the X-ray scattering and TEM results described above, it is possible to describe the sequence of processes that occurs during the crystallization of our blend systems and to relate each stage to the molecular composition of the system.

Shearing the melt results in the orientation of a small fraction of the material (orientation parameter $\langle P_2 \rangle \sim 0.01$ [30]), which corresponds to the very longest molecules within the system [5,31,41]. On cooling, these structures form 'thread-like precursors' [43] for the contiguous shish-kebab cores, which, themselves, serve as nucleation sites for subsequent chainfolded crystallization. In this way, an oriented lamellar texture develops from an, initially, largely unoriented linear molecular fraction within the melt. Isothermal crystallization continues until the minority of crystallizable material is exhausted, to leave a fully relaxed melt that is rich in branched material.

Despite being unoriented, crystallization of this majority fraction, nevertheless, leads to further oriented crystallization as a result of the presence of the pre-established oriented framework. This process, by which an unoriented molecular melt is mapped onto an oriented lamellar texture, we have termed templating; previously, this same term has been used to describe the far more direct process by which 'kebab' lamellae form upon extended shish structures (see, for example, Ref. [10]). At present, the precise mechanisms through which a quiescent BPE melt rapidly evolve into an oriented morphology as a consequence of the presence of a neighbouring oriented lamellar texture is unclear. Nevertheless, a degree of speculation is possible.

(i) Co-crystallization during the isothermal phase will result in the incorporation of the more linear sequences of the BPE into the isothermal lamellae. The resulting molecular cilia may, subsequently, serve as sites that are able to initiate BPE crystallization on cooling, as proposed in the quiescent case [55].
(ii) Alternatively, growth of the isothermal LPE lamellar growth-front may restart as soon as the thermodynamic conditions are commensurate with the linear segment distribution present within the melt.
(iii) Finally, crystallization of the BPE may simply occur from between the LPE lamellar framework with no specific crystallographic continuity, whereupon, the orientation seen in both our X-ray scattering and TEM data is simply a consequence of crystallization with such a confined geometry.

Whatever the precise mechanism, the principle is, nevertheless, clear. Evolution of the overall microstructure is not determined equally by each molecular fraction within the melt but, rather, gross changes in microstructure (e.g. spherulitic to oriented lamellar) can be induced through relatively small changes in the molecular composition of the melt. Indeed, Kornfield et al. [18] have reported the development of oriented morphologies in polypropylene blends with a bimodal molecular mass distribution, which were prepared by adding a small fraction of high molecular mass material to a relatively low molar mass system. In contrast to the materials considered here, neither of these polypropylene grades was, in isolation, reported to produced oriented structures. Evidently, the precise molecular interactions that occur during shear in polydisperse, technological polymers are subtle and, consequently, fine tuning the molecular composition of a polymer presents extensive potential as a means of modifying morphological evolution and, thereby, optimizing the properties of polymeric materials to suit demanding applications. These results also have implications for the interpretation and, indeed, the design of small angle neutron scattering experiments containing deuterium labelled and unlabelled polyethylenes. We will report on such experiments at a later date.

5. Conclusions

The above study has applied a combination of in situ and ex situ techniques to the study of the crystallization behaviour of sheared polyethylene blends. This strategy was adopted to reduce overall crystallization rates, to aid real time scattering experiments, and to produce open morphologies that are more amenable to interpretation. Both scattering techniques and TEM indicate that the BPE used in this investigation does not form anisotropic structures when exposed to melt shear rates up to 30 s^{-1}. Conversely, the linear polyethylene displayed many of the characteristic forms of behaviour that we have previously reported. These include negligible anisotropy in the melt, a critical shear rate for oriented crystallization and, subsequently, the formation of classical shish-kebabs. The primary objective of blending was to study the formation of these structures and, initially, it was envisaged that the majority matrix would simply behave as a stress transfer medium. Unexpectedly, it also was found to become oriented when crystallized in the presence of oriented LPE shish-kebabs. This process, which we have termed templating, demonstrates that the crystallization behaviour of the bulk of a polydisperse system can be dramatically changed through the addition of particular molecular fractions. At present, we are unable to identify the underlying mechanism by which templating occurs but it is, nevertheless, clear that gross changes in microstructure, and consequently properties, may be induced by

appropriately tuning the molecular composition of the melt and the imposed processing conditions.

Acknowledgements

This work was performed as part of the Royal Society, Academica Sinica funded link between The University of Reading and the Institute for Applied Chemistry, Changchun. The synchrotron radiation based experiments were performed at the CCLRC Daresbury Laboratory and we thank Anthony Gleeson for his assistance on the beam-line. JJH acknowledges the support of EPSRC and BP Chemicals snc through a CASE award. We thank BP Chemicals and Borealis Polymers for the supply of the linear and branched polyethylenes.

References

[1] Somani RH, Hsiao BS, Nogales A, Srinivas S, Tsou AH, Sics I, et al. Macromolecules 2000;33:9385.
[2] Kumaraswamy G, Verma RK, Issaian AM, Wang P, Kornfeld JA, Yeh F, et al. Polymer 2000;41:8931.
[3] Somani RH, Hsiao BS, Nogales A, Fruitwala H, Srinivas S, Tsou AH. Macromolecules 2001;34:5902.
[4] Nogales A, Hsiao BS, Somani RH, Srinivas S, Tsou AH, Balta-Calleja FJ, et al. Polymer 2001;42:5247.
[5] Seki M, Thurman DW, Oberhauser JP, Kornfield JA. Macromolecules 2002;35:2583.
[6] Yamazaki S, Hikosaka M, Toda A, Wataoka I, Yamada K, Tagashira K. J Macromol Sci, Part B: Phys 2003;B42:499.
[7] Agarwal PK, Somani RH, Weng W, Mehta A, Yang L, Ran S, et al. Macromolecules 2003;36:5226.
[8] Chai CK, Auzoux Q, Randrianatoandro H, Navard P, Haudin J-M. Polymer 2003;44:773.
[9] García Gutiérrez M-C, Alfonso GC, Riekel C, Azzurri F. Macromolecules 2004;37:478.
[10] Kumaraswamy G, Verma RK, Kornfield JA, Yeh F, Hsiao BS. Macromolecules 2004;37:9005.
[11] Peterlin A. Pure Appl Chem: Macromol Chem 1973;8:277.
[12] Peterlin A. Midland macromolecular monographs. In: Miller RL, editor. Flow-induced crystallization in polymer systems, Vol. 6. New York: Gordon and Breach Science; 1979 pp.1–29.
[13] Keller A, Machin MJ. J Macromol Sci, Phys Ed (B) 1967;1:41.
[14] Hay JN, Keller A. J Mater Sci 1967;2:538.
[15] Ulrich RD, Price FP. J Appl Polym Sci 1976;20:1077.
[16] Hsiue ES, Robertson RE, Yeh GSY. Polym Eng Sci 1983;23:74.
[17] Yang L, Somani RH, Sics I, Hsiao BS, Kolb R, Fruitwala H, et al. Macromolecules 2004;37:4845.
[18] Kornfield JA, Kumaraswamy G, Issaian AM. Ind Chem Res 2002;41:6383.
[19] Janeschitz-Kriegl H. Colloid Polym Sci 2003;281:1157.
[20] Somani RH, Yang L, Hsiao BS, Fruitwala H. J Macromol Sci, Part B: Phys 2003;3-4:515.
[21] Bassett DC, Hodge AM. Proc R Soc Lond A 1981;377:25.
[22] Bassett DC, Hodge AM, Olley RH. Proc R Soc Lond A 1981;377:39.
[23] Conde Braña MT, Iragorri Sainz JI, Terselius B, Gedde UW. Polymer 1989;30:410.
[24] Keith HD, Padden FJ. J Appl Phys 1964;35:1270.
[25] Keith HD, Vadimsky RG, Padden FJ. J Polym Sci A-2 1970;8:1687.
[26] Vaughan AS. Polymer 1992;33:2512.
[27] Hill MJ, Barham PJ, Keller A, Rosney CAA. Polymer 1991;32:1384.
[28] Kyu T, Hu S-R, Stein RS. J Polym Sci, Part B: Polym Phys 1987;25:89.
[29] Minick J, Moet A, Baer E. Polymer 1995;36:1923.
[30] Pople JA, Mitchell GR, Chai CK. Polymer 1996;37:4187.
[31] Pople JA, Mitchell GR, Sutton SJ, Vaughan AS, Chai CK. Polymer 1996; 37:4187.
[32] Mitchell GR, Andresen EM. Scattering from polymers. In: Cebe P, Hsiao BS, Lohse DJ, editors. ACS symposium series 739. Washington DC, USA: American Chemical Society; 1999. pp. 390–404.
[33] Nogales A, Thornley SA, Mitchell GR. J Macromol Sci Phys 2004;B34: 1161.
[34] Pople JA, Mitchell GR, Chai CK. Adv X-ray Anal 1995;38:531.
[35] Pople JA, Keates PA, Mitchell GR. J Synch Rad 1997;4:267.
[36] Olley RH, Hodge AM, Bassett DC. J Polym Sci, Polym Phys Ed 1979;17: 627.
[37] Vaughan AS. Sci Prog Oxford 1992;76:1.
[38] Olley RH, Bassett DC. Polymer 1982;23:1797.
[39] Willison JHM, Rowe AJ. In: Glauert AM, editor. Replica, shadowing and freeze-etching techniques, practical methods in electron microscopy, Vol. 8. North Holland: Amsterdam; 1980.
[40] Hosier IL, Vaughan AS, Swingler SG. J Mater Sci 1997;32:4523.
[41] Heeley EL, Morgovan AC, Bras W, Dolbnya IP, Gleeson AJ, Ryan AJ. Phys Chem Commun 2002;5:158.
[42] Moitzi J, Skalicky P. Polymer 1993;34:3168.
[43] Jay F, Haudin JM, Monasse B. J Mater Sci 1999;34:2089.
[44] Liedauer S, Eder G, Janeschitz-Kriegl H. Intern Polym Proc 1995;10:243.
[45] Keller A. J Polym Sci 1955;25:31.
[46] Keller A, Kolnaar HWH. Processing of polymers. In: Meijer HEH, editor. Materials science and technology. Materials science and technology, Vol. 18. Darmstadt: VCH; 1997. pp. 310–405.
[47] Holt JJ, Mitchell GR. Submitted to J Macromol Sci Phys B.
[48] Song HH, Stein RS, Wu D-Q, Ree M, Phillips JC, LeGrand A, et al. Macromolecules 1988;21:1180.
[49] Gohil RM, Phillips PJ. Polymer 1986;27:1687.
[50] Janimak JJ, Stevens GC. Polymer 2000;41:4233.
[51] Hosier IL, Bassett DC, Moneva IT. Polymer 1995;36:4197.
[52] Bashir Z, Odell JA, Keller A. J Mater Sci 1984;19:3713.
[53] Bashir Z, Odell JA, Keller A. J Mater Sci 1986;21:3993.
[54] Puig CC. Polymer Bull 1996;36:361.
[55] Puig CC. Polymer Bull 1997;38:715.